Polymer Degradation and Stability 200 (2022) 109943

Contents lists available at ScienceDirect

Polymer Degradation and Stability

journal homepage: www.elsevier.com/locate/polymdegradstab

Strategies to mitigate the synergistic effects of moist-heat aging on TEMPO-oxidized nanocellulose☆

Camilla H.M. Camargos[a,b], Giovanna Poggi[b], David Chelazzi[b], Piero Baglioni[b], Camila A. Rezende[a,*]

[a] Physical Chemistry Department, Institute of Chemistry, University of Campinas – UNICAMP, Campinas, SP 13083-970, Brazil
[b] CSGI and Chemistry Department, University of Florence, Via della Lastruccia 3, Sesto Fiorentino, FI 50019, Italy

ARTICLE INFO

Article history:
Received 14 February 2022
Revised 12 April 2022
Accepted 16 April 2022
Available online 18 April 2022

Keywords:
Cellulose nanofibril
Cellulose nanocrystal
Lignin nanoparticle
Accelerated aging
Thermal stability
DPPH scavenging

ABSTRACT

Cellulose oxidation catalyzed by TEMPO ((2,2,6,6-tetramethylpiperidin-1-yl)oxyl) is a trending methodology to enable the fibrillation and production of large amounts of cellulose nanofibrils (CNF) in a cost-effective and energy-saving manner. However, TEMPO-oxidized CNF lack colorimetric, thermal, and physicochemical stability due to intrinsic structural characteristics, i.e., the presence of sodium carboxylate functional groups and anhydroglucuronate units of low molecular weight. The susceptibility of CNF to deterioration at moist-heat conditions can negatively impact the use of these promising nanomaterials in long-term applications, such as protective coatings and electronic devices. Herein, we showed that the incorporation of lignin nanoparticles (LNP) enhanced the resistance to degradation of nanocomposite films based on nanocelluloses (CNF and cellulose nanocrystals). The improvement of the aging performance in nanolignin-containing films was attributed to the higher antioxidant capacity provided by lignin, which also imparted UV-protection. Alternatively, the removal of unstable functional groups and residues in TEMPO-oxidized CNF by an alkali-acid post-treatment was also proven effective in imparting higher thermal, physicochemical, and colorimetric stability to CNF and nanocomposite films. Therefore, the incorporation of LNP or the implementation of a post-treatment protocol into CNF are diverse, yet simple and efficient strategies to enable the application of these bio-based green nanomaterials into durable products.

1. Introduction

Bio-based nanostructures, such as cellulose nanofibrils (CNF) and nanocrystals (CNC), are promising candidates for the development of advanced materials [1,2]. Potential middle to long-term applications include the development of waterborne coatings [3,4] and consolidants [5–7], packaging materials with barrier properties [8,9], membranes for environmental remediation [10,11], electronic devices [12], and tissue engineering scaffolds based on or incorporated with CNF or CNC [13].

While needle-shaped CNC are typically obtained by sulfuric acid hydrolysis [2,14], CNF are filament-like nanostructures produced by the mechanical fibrillation of cellulosic pulps. In general, enzymatic hydrolysis or TEMPO-mediated oxidation are performed before refining, homogenization, blending and/or ultrasonication steps to overcome the strong intermolecular forces within the fibers [14]. Through TEMPO-catalyzed oxidation, C6 primary hydroxyl groups on cellulose are regioselectively converted into carboxylate groups *via* aldehyde intermediates [1]. The introduction of anionically charged groups increases the electrostatic repulsion between the microfibrils in aqueous media and facilitates the mechanical nanofibrillation [15], reducing the required energy input.

Due to their cost-effective production and tailored morphological and surface properties, TEMPO-oxidized CNF have been explored for plenty of target applications. For example, these nanostructures were applied as coatings to strengthen paper substrates [3,16] or to protect copper electrodes against short-circuits [17]. Additionally, these nanostructures were used as suitable platforms for the facile synthesis of calcium hydroxide nanoparticles with controlled rheological properties intended for cultural heritage conservation [18]. Notwithstanding the benefits of performing TEMPO-mediated oxidation to obtain nanofibrils with high yields [19], this carboxylation method can bring some drawbacks for the applications, such as the remarkable yellowing of CNF upon oven-drying at high temperatures [14,20–23].

☆ Submitted to Polymer Degradation and Stability

* Corresponding author at: Institute of Chemistry, UNICAMP: Universidade Estadual de Campinas, 13083-970 Campinas, São Paulo, Brazil.
E-mail address: camilaiq@unicamp.br (C.A. Rezende).

https://doi.org/10.1016/j.polymdegradstab.2022.109943
0141-3910/

Takaichi and co-workers [21] attributed the color change of TEMPO-oxidized CNF to the presence of ketones in cellulose C2 and C3, while Xia et al. [22] and Mishra et al. [23] attributed the appearance of yellow-to-brown tinted degradation products to the presence of unconverted aldehydes in cellulose C6. Furthermore, TEMPO-catalyzed oxidation has been documented to produce thermally unstable sodium carboxylate groups [24] and low molecular weight sodium anhydroglucuronate units that remain incorporated into the oxidized cellulose moieties [25].

In the long-term and/or under harsh thermal conditions, the lack of resistance to degradation becomes a problem for numerous end-uses, potentially preventing the utilization of CNF prepared *via* TEMPO-oxidation. For instance, applications such as coatings for works of art or transparent papers for electronic devices require durable CNF products to withstand harsh conditions without tinting or thermally decomposing [12]. As the instability of TEMPO-CNF should not preclude the further use of such advantageous bio-based nanomaterials, some strategies have been introduced to improve their thermochemical stability. An alternative is the implementation of post-treatments for further oxidation [23], as well as reduction [26], methylation [25], and polymer grafting [27]. Herein, we extensively investigated the stabilization of TEMPO-CNF nanocomposites, considering a chemical post-treatment and, alternatively, a novel, greener protocol using nanolignin.

Given the benefit of combining cellulose nanostructures with different morphologies to produce tailored all-nanocellulose systems [28], we blended elongated, flexible TEMPO-oxidized CNF with shorter, rigid CNC to obtain transparent films. As the addition of highly crystalline CNC alone only slightly improved the aging behavior of the CNF-based systems, we then introduced an alternative stabilization approach by incorporating lignin nanoparticles (LNP) to prepare sustainable nanocomposite films. LNP are highly antioxidant and can also provide UV-protection ability to polymeric matrices, such as poly(vinyl alcohol) [29]. Moreover, while combinations of CNF with spherical LNP [30,31] or CNC with solubilized lignin [32] have been previously reported, the development of ternary CNF/CNC/LNP nanocomposite films and the contribution of LNP to the stability of TEMPO-oxidized CNF have not been addressed so far.

In this regard, we performed a comprehensive study on the artificially-accelerated aging of single-component and transparent ternary nanocomposites based on TEMPO-oxidized CNF under variable hydrothermal conditions to evaluate the synergistic influence of temperature and relative humidity on the stability of self-standing films. We assessed alterations in color, crystallinity, thermal behavior, and degree of polymerization (DP), as well as the capability of the films to scavenge DPPH free radicals. Furthermore, using Fourier-transform infrared (FTIR) spectroscopy and 2D mapping (micro-FTIR), thermogravimetric analysis (TGA), as well as DP and colorimetric measurements, we indirectly confirmed the pivotal role played by sodium carboxylate groups in the poor degradation resistance of TEMPO-oxidized nanocellulose. Although the presence of such chemical structures has already been mostly correlated with CNF thermal instability, the results provided here demonstrated for the first time the major contribution of sodium carboxylate moieties also to the colorimetric and chemical changes undergone by TEMPO-oxidized CNF upon aging. A sequential alkali-acid post-treatment was conducted to efficiently remove these functional groups and simultaneously increase the colorimetric, chemical, and thermal stability of CNF, pairing the performance of single-component CNF and nanolignin-containing nanocomposite films. Thus, we propose both the chemical post-treatment and the LNP incorporation as diverse, interesting, and facile strategies to preserve the integrity and visual aspect of products containing TEMPO-oxidized CNF.

2. Materials and methods

2.1. Chemicals and materials

Acetone (P.A.), 1,4-dioxane (P.A.), ethanol (P.A.), methanol (P.A.), sodium bromide (NaBr, P.A.), sodium hydroxide (NaOH, 98%), and sulfuric acid (H_2SO_4, 95–98%) were purchased from Synth (Diadema, Brazil). Bis(ethylenediamine)copper(II) hydroxide solution (CED, 1 mol L^{-1}), 1,1-di(phenyl)-2-(2,4,6-trinitrophenyl)hydrazine (DPPH), and (2,2,6,6-tetramethylpiperidin-1-yl)oxyl radical (TEMPO, 98%) were purchased from Sigma-Aldrich (St. Louis, USA). Sodium chlorite (NaClO, 10–12%) was obtained from Êxodo Científica (Sumaré, Brazil).

Elephant grass (*Pennisetum purpureum*) was kindly provided by the Institute of Animal Science (Instituto de Zootecnia–SP, Nova Odessa, Brazil). Plants (leaves and stems) were hydrothermally pretreated with diluted H_2SO_4 and NaOH to isolate cellulose fibers and lignin, according to previously reported procedures [28,29].

2.2. Preparation and morphological characterization of cellulose and lignin nanostructures

CNF were prepared by TEMPO-mediated oxidation with NaBr/NaClO in water followed by sonication, while CNC were obtained by conventional acid hydrolysis with concentrated H_2SO_4. CNF were extracted from cellulose fibers obtained from both the leaves and stems of elephant grass, while CNC were obtained from leaves only. These precursor cellulose fibers contained *ca.* 80% (w/w) cellulose, 8–12% (w/w) lignin, and 3–4% (w/w) hemicellulose. A detailed description of the methodology used to produce the nanocelluloses and their complete characterization were published before [28]. CNF and CNC presented, respectively, *ca.* 3 and 4% (w/w) of residual lignin. In aqueous dispersions, the zeta potential at pH 7 and the concentration of ionizable groups on the surface were, respectively, – 50 mV and 0.62 mmol g^{-1} of CNC (sulfate half-ester groups) and up to –76 mV and 1.6 mmol g^{-1} of CNF (carboxylic acid/sodium carboxylate groups). The morphology of nanocelluloses was assessed by Transmission Electron Microscopy (TEM) in a Carl Zeiss LIBRA 120 microscope (Oberkochen, Germany) using bright field mode. Aqueous dispersions of CNC or CNF (concentration: 10 μg mL^{-1}) were deposited on 400 mesh carbon-coated copper grids and stained with 2% (w/v) uranyl acetate. Samples were dried in a desiccator at room temperature for at least 4 h prior to analysis.

LNP were prepared by a nanoprecipitation method using the lignin extracted from elephant grass leaves. Bulk lignin was solubilized in acetone solution and water was added as an antisolvent. A detailed description of the methodology used to produce and characterize these LNP can be found elsewhere [29]. In aqueous dispersion, LNP presented zeta potential of –46 mV at pH 7 and a content of ionizable groups of 1.63 mmol g^{-1} (phenolic hydroxyl and carboxylic acid groups). Scanning electron microscopy (SEM) images of LNP were acquired in a Quanta FEG 250 microscope (FEI, Hillsboro, USA) operating at 5 kV (secondary electron detector). LNP dispersion (concentration: 10 μg mL^{-1}) was deposited on a clean mica substrate and sputter coated with iridium in a BAL-TEC MED 020 sputter coater (Balzers, Liechtenstein) operating at 11.3 mA for 120 s.

2.3. Post-treatment of oxidized cellulose fibers

When highlighted, TEMPO-oxidized fibers (before sonication/fibrillation) underwent an alkali-acid post-treatment, adapting previously reported procedures [25,27]. To remove sodium anhydroglucuronate units, the aqueous slurry of oxidized cellulose fibers (~1% w/w, 100 mL) was treated with 100 mL of 1 mol L^{-1}

Table 1
Formulation of single-component and nanocomposite films.

Film	CNF* % (w/w)	CNC% (w/w)	LNP% (w/w)
CNF	100	0	0
CNC	0	100	0
CNF/CNC	66	34	0
CNF/CNC/LNP1	65	34	1
CNF/CNC/LNP5	60	35	5
CNF/CNC/LNP10	60	30	10
CNF/CNC/LNP25	50	25	25

* To produce single-component and nanocomposite films with improved tensile strength and Young's modulus, CNF from leaves and stems were combined in a 2:1 ratio in all experiments, according to a previous work [28].

NaOH at approximately 100 °C in a silicone oil bath for 150 min under constant stirring (400 rpm). Then, to convert sodium carboxylate into free carboxyl groups, oxidized fibers were treated with 100 mL of 0.1 mol L^{-1} HCl at room temperature for 120 min under constant stirring. After each step, the pulp was washed 5 times with deionized water *via* centrifugation at 3500 rpm for 10 min. A color change from white to yellow/brown was observed during the first step, and the slurry turned white/colorless again after the rinsing steps. A reduction in the amount of remaining solid fibers is expected. The post-treated pulp was then sonicated to yield fibrillated CNF. The zeta potential of post-treated CNF in water was evaluated in triplicate using a Malvern Zetasizer® Nano ZS-Zen 3600 (Malvern, UK), being measured as – 55 ± 4 mV (leaves) and – 51 ± 3 mV (stems). The concentration of ionizable groups (weak acid, carboxylic acid groups) was assessed by conductometric titration following a previously reported protocol [28], resulting in contents of 0.87 ± 0.02 mmol g^{-1} of post-treated CNF from leaves and 0.84 ± 0.01 mmol g^{-1} of post-treated CNF from stems.

2.4. Preparation of single-component and nanocomposite films based on nanocellulose

Self-standing films containing 0 to 25% (w/w) of LNP and 75 to 100% (w/w) of nanocellulose (untreated or post-treated CNF and/or CNC) were formulated according to Table 1. In all nanocomposite formulations, the proportional weight ratio between CNF and CNC contents was approximately 2:1. This proportion was selected after several trials, considering film malleability, flatness, and uniformity. Stock aqueous dispersions of each component were blended, and deionized water was added to maintain a fixed final volume (16 mL) and concentration (4 mg mL^{-1}). The same amounts were used to produce single-component CNF or CNC films, as well as binary CNF/LNP and CNC/LNP nanocomposites (1 or 10% (w/w) LNP). The dispersions were homogenized using probe-sonication (4 mm tip) with a 220 W output power for 2 min and underwent solvent casting in polystyrene dishes with a 64-cm^2 area. Films were dry and detached from the casting dish after *ca.* 72 h of drying at 25 °C and 50% relative humidity. The dry weight of these films was approximately 64 mg, corresponding to an average weight-to-area ratio of 1 mg cm^{-2}.

2.5. Artificially-accelerated aging

Single-component and selected nanocomposite films underwent artificial accelerated aging inside airtight flasks kept in an oven at 40 or 80 °C for 168 h. Simultaneously, relative humidity (~0% (dry), 25%, 50%, or 75% RH) was controlled inside the flasks using calcium chloride (RH <10%) or glycerol aqueous solutions (94% (w/w) = 25% RH; 80% (w/w) = 50% RH; 58% (w/w) = 75% RH) [33] and assessed using a thermohygrometer. The experimental setup is depicted in Fig. S1. Nanocomposites containing post-treated TEMPO-oxidized CNF were aged exclusively at moist-heat condition (80 °C and ~75% RH) [34,35].

2.6. Characterization of unaged and aged nanocellulose-based films

2.6.1. Thickness measurements

The average thickness of single-component and nanocomposite self-standing films was measured using a Digimatic Micrometer (Mitutoyo Corporation, Kanagawa, Japan) with a reading error of 1 μm. Measurements were performed in at least ten random regions of each film in triplicate. Film average thickness is presented in Table S1.

2.6.2. Diffuse reflectance spectroscopy (DRS)

DRS spectra of the films were collected in the range of 200–800 nm, with a 0.5 nm spectral resolution, using a Shimadzu UV-2450 DRS spectrophotometer (Kyoto, Japan) in transmittance mode.

2.6.3. Colorimetric measurements

Colorimetric coordinates in the CIEL*a*b* color space were assessed by a portable X-RITE SP60 VIS spectrophotometer (Grand Rapids, USA) with integration sphere, using standard D65 illuminant and standard 10° observer. The color difference (ΔE) [36] between unaged and aged films was calculated according to Eq. (1):

$$\Delta E = \sqrt{(\Delta L^*)^2 + (\Delta a^*)^2 + (\Delta b^*)^2} \quad (1)$$

where ΔL*, Δa* and Δb* are the variation, respectively, in the coordinate of lightness/darkness L* (+ light, – dark), in the component red/green a* (+ red, – green), and in the component yellow/blue b* (+ yellow, – blue). During measurements, films were placed on a homogeneous white surface with colorimetric parameters: L* = 92.5 ± 0.1; a* = 1.3 ± 0.1; b* = – 6.2 ± 0.4. All measurements were performed in six replicates at least. Tolerance criteria accepted here indicates that at ΔE < 3.5, a standard observer does not perceive color difference between two samples; at 3.5 < ΔE < 5, an observer perceives significant color difference between two samples; and that when ΔE > 5, an observer perceives two distinct colors [36].

2.6.4. Thermogravimetric analysis (TGA)

TGA and DTG (derivative thermogravimetry) curves of CNF and CNC single-component films, as well as nanocomposite films were obtained in a SDT Q600 apparatus (TA Instruments, New Castle, USA). Self-standing films were scissor-cut, 3 mg were placed in a clean crucible, then heated under nitrogen flow from room temperature to 800 °C at a 10 °C min^{-1} heating rate. The experimental error was ± 2 °C. By convention, all thermograms were corrected so that weight loss in temperatures lower than 100 °C was disregarded [27]. The thermal decomposition temperature (T_d) was defined as the temperature at which the mass decreased by 5% in the TGA curve and the maximum decomposition temperature (DTG_{peak}) was defined as the temperature at the maximum peaks of the DTG curve [25].

2.6.5. Differential scanning calorimetry (DSC)

DSC curves of self-standing films were obtained in a DSC Q100 apparatus (TA Instruments). Samples were scissor-cut, *ca.* 5 mg were placed in a new crucible, heated under nitrogen flow from room temperature (25 °C) to 200 °C and then cooled to room temperature at a rate of 10 °C min^{-1}. Specifically for sample CNF/CNC/LNP10, containing 10% (w/w) LNP, a second assay was performed comprising a first heating to 200 °C at a rate of 10 °C min^{-1}, followed by cooling to 0 °C at 5 °C min^{-1} and a second heating to 200 °C at 10 °C min^{-1}.

2.6.6. Viscosimetric degree of polymerization (DP_v)

Standardized intrinsic viscosity (η) measurements were performed using Cannon-Fenske viscosimeters and a thermostatic water bath at 25 ± 1 °C [37]. 40 mg of film samples were dissolved in 20 mL of 0.5 mol L^{-1} CED at room temperature for 12 h and η was measured for duplicates three times with a stopwatch [26]. The relationship between DPv and η [38] was calculated using Eq. (2) and (3):

$$\eta = 0.42 \times DP_v, \text{ when } DP_v < 950 \quad (2)$$

$$\eta = 2.28 \times DP_v^{0.76}, \text{ when } DP_v > 950 \quad (3)$$

2.6.7. X-ray diffraction (XRD)

Diffractograms of film samples were collected in a Shimadzu XRD-6000 diffractometer using CuKα radiation generated at 40 kV and 30 mA, over a 2θ range of 5–50°, with scan speed of 2° min^{-1}. Crystallinity index (CrI) was measured using Eq. (4):

$$CrI = \frac{(I_{200} - I_{am})}{I_{200}} \quad (4)$$

where I_{200} refers to the crystalline cellulose (200) peak and I_{am} refers to the contribution of the amorphous halo [39]. Sample holder and background were adequately subtracted from the diffractograms.

2.6.8. FTIR spectroscopy

ATR-FTIR spectra of CNF and post-treated CNF films were collected in an Agilent Cary® 630 FTIR (Santa Clara, USA) using a spectral resolution of 4 cm^{-1} and 128 scans per run.

2.6.9. Micro-FTIR 2D mapping

FTIR imaging was performed with a Cary 670 FTIR spectrophotometer coupled to a Cary 620 FTIR microscope (Agilent Technologies), using a 15x Cassegrain objective. Measurements were carried out in reflectance mode over the gold-sputtered reflective slides, while background spectra were collected on a gold-plated surface. The experimental conditions were: spectral range of 3900–900 cm^{-1}, 128 scans for each acquisition, spectral resolution of 4 cm^{-1}, open windows. A 128 × 128 pixels Focal Plane Array (FPA) detector was used; the pixel size is 5.5 μm × 5.5 μm, and each pixel provides an independent spectrum from the sample surface. Each analysis delivers spectra of a 700 × 700 μm^2 "tile".

2.6.10. DPPH radical scavenging activity

Adapting previously reported procedures [29,40–42], the antioxidant activity of nanocomposite films was estimated as the percentage of DPPH radical scavenging activity using a colorimetric assay. Film samples (*ca.* 1 mg) were soaked in 1 mL of 90% (v/v) dioxane in a quartz cuvette for 3 h. Then, protected from direct light incidence, 2 mL of freshly prepared 65 μmol L^{-1} $DPPH^{\bullet}$ in methanol was added to the same cuvette. $DPPH^{\bullet}$ concentration immediately at the beginning (0 min) and after 16 and 30 min was tracked using the relative intensity of the absorption band at 515 nm collected in a Varian's Cary® 50 UV–Vis spectrophotometer. The percentage of DPPH radical scavenging activity was evaluated using Eq. (5):

$$\%Scavenging = \frac{(Abs\ blank) - (Abs\ sample)}{Abs\ blank} \times 100 \quad (5)$$

where *Abs blank* refers to the relative absorbance at 515 nm (λ_{max}) after 0, 16, and 30 min for systems containing only solubilized $DPPH^{\bullet}$ in methanol/dioxane; and *Abs sample* is the absorbance of each sample at the same specific time. All measurements were performed in duplicate at room temperature. For comparison, the same procedure was repeated replacing the solvents (methanol and dioxane) by ethanol in a greener and less toxic approach.

3. Results and discussion

3.1. Transparency, UV-absorbance, and colorimetric features of nanocellulose-based nanocomposites

CNF, CNC, and LNP were combined to produced nanocomposite films (Fig. 1). This approach relied on the natural, intrinsic chemical compatibility between cellulose and lignin at the nanometer level [43]. The morphology of these nanostructures, as observed by electron microscopy, is presented in Fig. 1A–D. CNF extracted from elephant grass leaves and stems presented elongated shape (Fig. 1A, B), with average length ranging from 600 to 1000 nm. CNC were rod-like nanoparticles (Fig. 1C) with shorter average length between 100–200 nm [28]. All nanocelluloses presented average diameter of 3–4 nm, while LNP showed spherical morphology (Fig. 1D) with an average diameter of *ca.* 50 nm [29]. As depicted in Fig. 1E, the surface chemistry of these nanostructures was characterized by the presence of sodium carboxylate groups onto CNF, sulfate half-ester groups onto CNC, and phenolic hydroxyls onto LNP.

Never-dried nanostructures were blended in aqueous dispersions and underwent casting to produce compact, bidimensional assemblies (Fig. 1E) in the form of self-standing, transparent films (Fig. 1F). While neat CNC usually results in rather brittle films [44], their incorporation here contributed to obtain flatter and more homogeneous CNF-based nanocomposite films. CNC and CNF single-component films, as well as films containing 0 and 1% (w/w) LNP were visually colorless. Films containing 5% (w/w) LNP or more presented a brownish coloration, from light brown in CNF/CNC/LNP5 and CNF/CNC/LNP10 to dark brown/yellow in CNF/CNC/LNP25.

DRS spectra showed that increasing lignin content imparted decreasing transmittance in both UV (200–400 nm) and visible ranges (400–800 nm) (Fig. 2A). Farooq et al. [31] observed similar concentration-dependence of optical transmittance in CNF films containing colloidal lignin or lignin powder. Here, single-component CNC and CNF, as well as CNF/CNC nanocomposite films were the most transparent in the visible range, while CNF/CNC/LNP10 and CNF/CNC/LNP25 presented the highest UV-photoabsorbance (Fig. 2B). However, the incorporation of 5 and 25% (w/w) LNP only provided a slightly greater contribution to the UV-shielding while considerably reducing the transparency in comparison to the incorporation of 1 and 10% (w/w) LNP, respectively. Therefore, CNF/CNC, CNF/CNC/LNP1, and CNF/CNC/LNP10 nanocomposites were considered the most applicable and selected for further studies.

Whereas single-component films of CNF and CNC, as well as CNF/CNC and CNF/CNC/LNP1 nanocomposites presented similar colorimetric parameters, the incorporation of 10% (w/w) LNP changed the colorimetry of the nanocellulose-based films (Fig. 2C). Colorimetric measurements in the CIEL*a*b* color space highlighted significant reductions in the L* (lightness) component, as well as increments in the yellow (+) contribution of the b* coordinate. In other words, the nanocomposite film with higher amount of LNP was darker and more yellowish. From the start, CNC film also presented a yellow hue due to the presence of *ca.* 4% (w/w) of residual lignin. Such colorimetric characteristics must be taken into consideration when applying these materials, for example in protective coatings.

3.2. Synergistic effect of moist-heat aging on the colorimetric deterioration of nanocellulose-based nanocomposite films

The performance of nanocellulose-based nanocomposites under several conditions of hydrothermal aging was assessed to study the

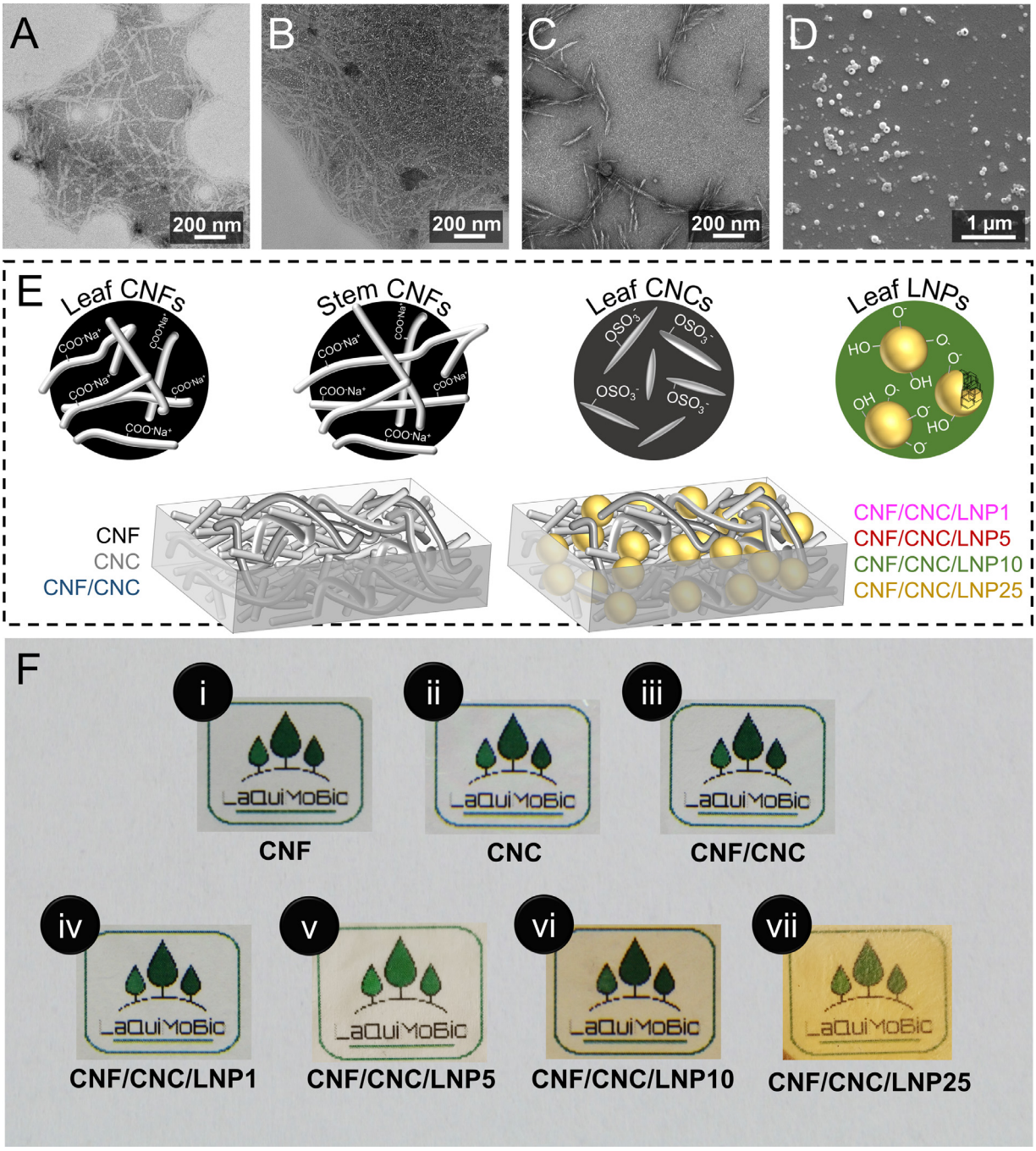

Fig. 1. TEM images of (A) leaf CNF, (B) stem CNF, and (C) leaf CNC. (D) SEM image of LNP. (E) Depiction of cellulose and lignin nanostructures and their corresponding single-component or nanocomposite films (compactly, two-dimensionally assembled). The main surface groups onto the nanoparticles are represented. The amphiphilic character of LNP is evidenced by the inner aromatic (hydrophobic) and outer hydroxyl groups (hydrophilic). (F) Photographs under visible light of single-component and nanocomposite films showing their transparency and color: (i) CNF, (ii) CNC, (iii) CNF/CNC, (iv) CNF/CNC/LNP1, (v) CNF/CNC/LNP5, (vi) CNF/CNC/LNP10, (vii) CNF/CNC/LNP25.

physicochemical stability of these films. Colorimetric changes were referred as phenomenological evidences of cellulose degradation [45]. No significant changes were observed in the visual aspect of the films aged at 40 °C for 168 h (Figs. 3A and S2). Indeed, dry and moist aging at a milder temperature imparted a color difference (ΔE) lower than the tolerance limit of 3.5 for all aged *versus* unaged samples (Fig. 3C). That is, no significant color change was perceived. Similarly, as showed in Fig. 3D, at dry conditions (~0% RH) the ΔE was within the tolerance limit of 3.5 for all CNF, CNC, and nanocomposite films aged at 80 °C. Also, no significant color difference was observed for films aged under low relative humidity (25%), except for CNF and CNF/CNC films.

At 80 °C, increasing relative humidity resulted in proportionally larger variation in the colorimetric parameters L* and b* (Fig. S3), entailing significant color difference after sample aging (Fig. 3D). This result highlights the synergistic action of high temperature and humidity to CNF degradation. The magnitude of the colorimetric degradation was directly dependent on the amount of moisture present in the aging atmosphere. A report by Graminski and coworkers [46] provided similar data on the deleterious effect of high temperature and increasing RH on the brightness reversion of cellulose paper.

Schedl et al. [47] showed that temperature and relative humidity – and the interaction between them – are the main fac-

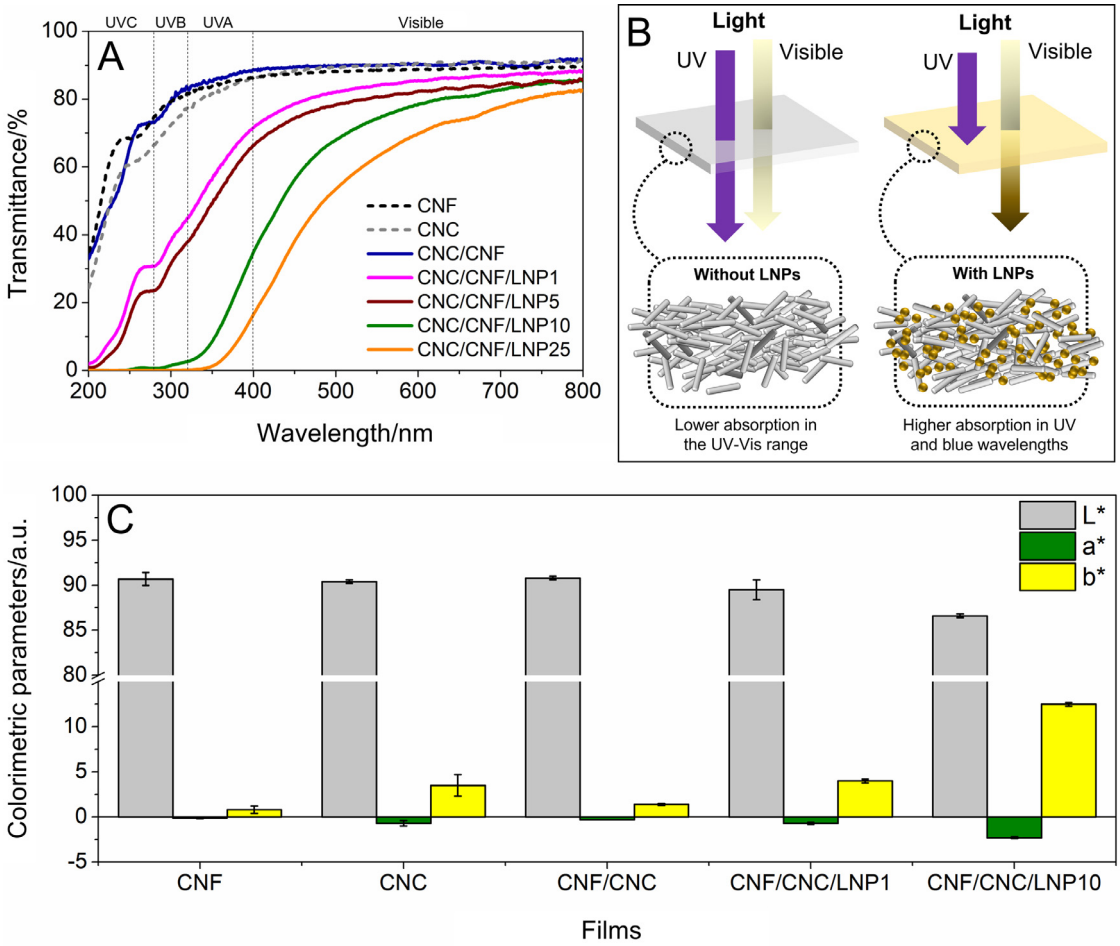

Fig. 2. (A) DRS UV-Vis spectra showing the transmittance pattern of single-component and nanocomposite films. (B) Depiction of the light absorbance of films containing lignin nanoparticles (LNP) or not. In the absence of nanolignin, the samples do not demonstrate substantial absorption either in the UV or visible range, while in the presence of nanolignin, the nanocomposites highly absorb in the UV and blue wavelengths [29], showing a yellow-to-brown coloration under visible light. (C) Colorimetric parameters of the films considering the CIEL*a*b* color space.

tors cooperating to the generation and further oxidation of key chromophores in paper samples. The combination of elevated temperature and humid air promotes the acceleration of degradative/oxidative pathways [48]. In addition to being a paramount reactant for acid hydrolysis which can occur in parallel to oxidation, water can act as: (i) a reaction medium and supplier of protons, radicals such as $HO^{\bullet}$, and other oxygen active species [49], (ii) a catalyst that accelerates the rate of cellulose degradation, (iii) a swelling agent that increases the available surface area for reactions, and (iv) a plasticizer that promotes molecular mobility [50].

Excluding neat CNC films, all the films showed $\Delta E > 5$ when aged at 80 °C with 50 or 75% RH for 168 h. Color changes were visually detected as darkening and yellowing (Fig. 3B), i.e., the browning of TEMPO-oxidized CNF and nanocomposite films. Yellowing phenomena are related to the arise of chromophores resulting from cellulose degradation products (Fig. S4A) due to thermal, oxidative, and hydrolytic stress reactions, specially under humid conditions [51,52]. By oxidative mechanisms, *via* hydroperoxides formed on cellulose C2, C3 and C6, hydroxyls can be converted into carbonyl groups (ketone on C2 and C3 or aldehyde on C6) [53,54], which are precursors of chromophores in cellulosic materials [51]. Further oxidation results in carboxyl groups, which catalyze the generation of such colored species.

Regarding TEMPO-oxidized celluloses, mainly carboxyl and few aldehyde groups on C6 are initially found in their structure [55]. Decarbonation of unconverted carbonyl or decarboxylation of sodium carboxyl groups on cellulose surface (Fig. S4B) have been indicated as the cause of the low thermal stability of the TEMPO-CNF [24,25]. Assuming that cellulose degradation by retro-aldol, redox, tautomerization, and decarboxylation proceeds at low rates even under ambient conditions due to the relatively low activation barriers of these reactions [56], we hypothesized that the latter mechanism likely took place in parallel pathways to oxidation. Under moist-heat aging, the decarboxylated products, unsaturated species from glucuronic acids (or sodium glucuronate units), could subsequently become additional chromophores.

Notwithstanding the general color difference, the colorimetric parameters of the film containing 10% (w/w) LNP underwent the smallest relative changes among the samples. For CNF/CNC/LNP10, the values of L* decreased from 87 ± 3 to 81 ± 4, while b* increased from 12 ± 5 to 18 ± 7. On the other hand, the film containing only TEMPO-oxidized CNF endured major changes: L* reduced from 90.7 ± 0.7 to 80 ± 3 and b* increased from –6 ± 1 to 17 ± 3. The remarkable contribution of nanolignin in mitigating the colorimetric changes of TEMPO-oxidized CNF-based nanocomposites was also confirmed by the ΔE of aged binary systems containing only commercial CNF and LNP, which was lower than that of single-component CNF (Fig. S5). In turn, the presence of LNP did not affect the stability of binary films of commercial CNC and LNP as compared to single-component CNC. Schmidt et al. [57] showed that lignin was able to inhibit the autoxidative degradation of lignin-containing cellulose pulps, preventing

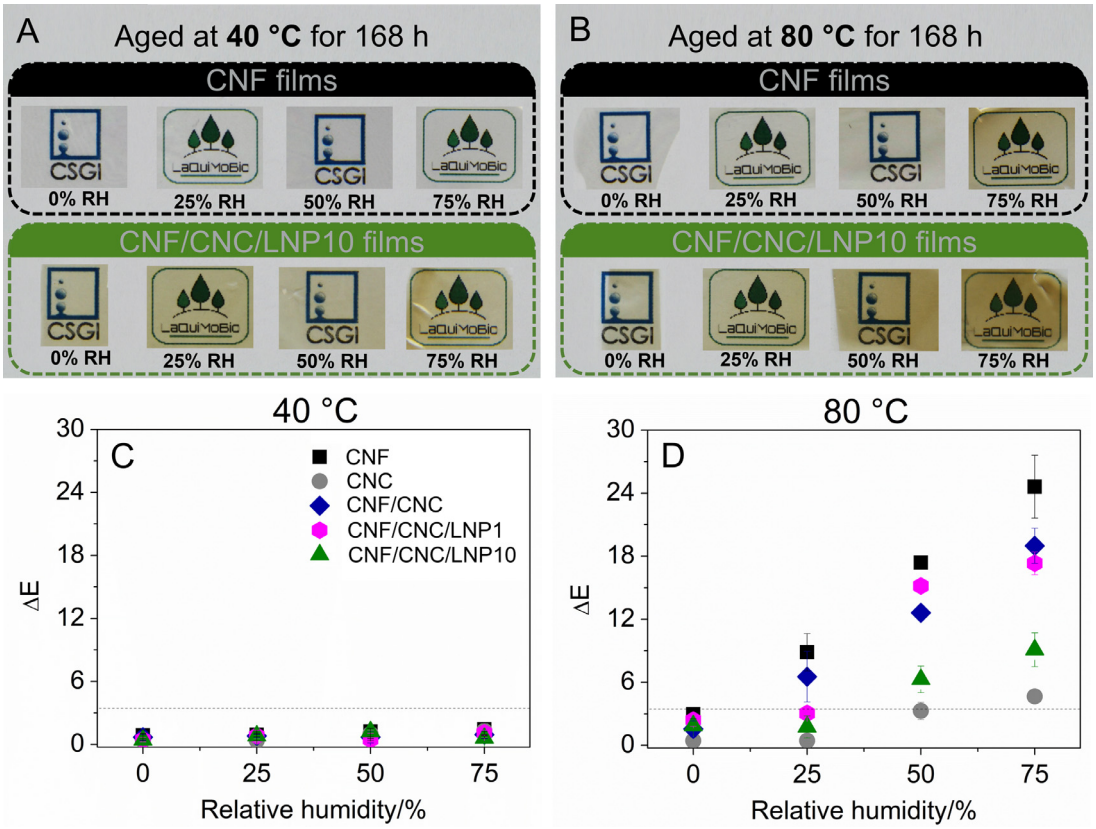

Fig. 3. Photographs under visible light of single-component CNF and CNF/CNC/LNP10 nanocomposite films aged at (A) 40 °C or (B) 80 °C under several relative humidities for 168 h. ΔE of the films before and after 168 h of artificial aging at (C) 40 °C and (D) 80 °C as a function of the relative humidity (~0 to 75%). Dotted lines indicate ΔE = 3.5.

strength loss, but suffering major discoloration. Under moist-heat conditions, the polyphenols present in lignin, as radical scavengers, can protect the cellulose by capturing active species sourced by water molecules [49] (Fig. S4C). Therefore, the antioxidant action and color stability of LNP probably contributed to better control yellowing in the LNP-containing nanocomposites by scavenging and stabilizing degradative radicals and oxygen active species.

In addition to the initial color of the single-component and nanocomposite films, colorimetric variations that arise over time due to exposure to environmental conditions must be considered in diverse and potentially long-lasting applications, for instance in protective coatings, papers, paints, and flexible electronic devices. While the application of a coating based on CNF/CNC/LNP10 may change the initial color of coated substrates, this layer will potentially remain stable over the coating lifespan. In contrast, the application of a coating composed solely of TEMPO-oxidized CNF (without LNP) could not imply an immediate change in the original coloration of the coated substrate, but such a coating would likely face major colorimetric changes over time, especially under harsh environmental conditions.

3.3. Effect of the incorporation of nanolignin on the thermal and chemical stability of nanocellulose-based nanocomposite films

TGA curves showed that TEMPO-oxidation reduced the decomposition temperature (T_d) of cellulose from 286 °C in the cellulose fibers (precursor used to produce CNF and CNC) to 217 °C in the CNF film (Fig. 4A). Furthermore, cellulose fibers and CNC films presented single maximum weight loss temperatures at *ca.* 358 °C and 302 °C, respectively, while the DTG curves of CNF films were broader, presenting two peaks centered at 243 °C and 309 °C (Figs. 4B). Fukuzumi and co-workers [25] ascribed comparable decomposition behavior to the decarbonation/decarboxylation of thermally unstable sodium anhydroglucuronate units present in TEMPO-oxidized CNF, which were absent in both the cellulosic precursor and CNC.

Table 2
Initial decomposition temperatures (T_d), referring to 5% weight loss in the TGA curves, and maximum weight loss temperatures (DTG_{peak}) of unaged and aged films (80 °C and 75% RH for 168 h). TGA and DTG measurements were performed under nitrogen flow.

Film	T_d/°C	$DTG_{peak(1)}$/°C	$DTG_{peak(2)}$/°C
Unaged CNF	217	243	309
Aged CNF	205	229	301
Unaged CNC	274	302	-
Aged CNC	273	307	-
Unaged CNF/CNC	221	246	318
Aged CNF/CNC	224	244	317
Unaged CNF/CNC/LNP1	224	248	313
Aged CNF/CNC/LNP1	226	248	321
Unaged CNF/CNC/LNP10	225	249	316
Aged CNF/CNC/LNP10	230	256	321

Table 2 summarizes the T_d and DTG_{peak} of unaged and aged samples. Films containing CNC and LNP (Fig. 5B and S6) were more thermally stable than single-component CNF films (Fig. 5A). Moreover, moist-heat aging slightly decreased the T_d of CNF film from 217 to 205 °C and shifted both DTG_{peaks} to lower temperatures. On the other hand, the harsh hydrothermal aging did not negatively influence the thermal behavior of single-component CNC or nanocomposite films. The overall increase in the thermal stability of CNF/CNC/LNP10 after aging could be attributed to the recrystallization of cellulose in this sample, as indicated by the XRD and DSC analyses that will be discussed shortly.

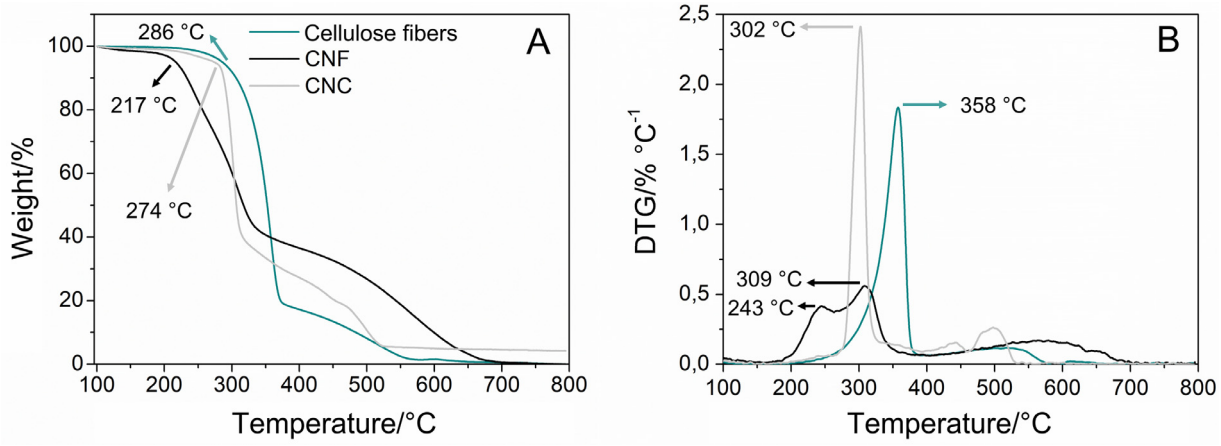

Fig. 4. Curves of (A) TGA and (B) corresponding DTG for the cellulose fibers and films of CNF and CNC for comparison. T_d (decomposition temperature) is indicated in (A) and the maximum decomposition temperatures (DTG_{peak}) are indicated in the DTG curves in (B).

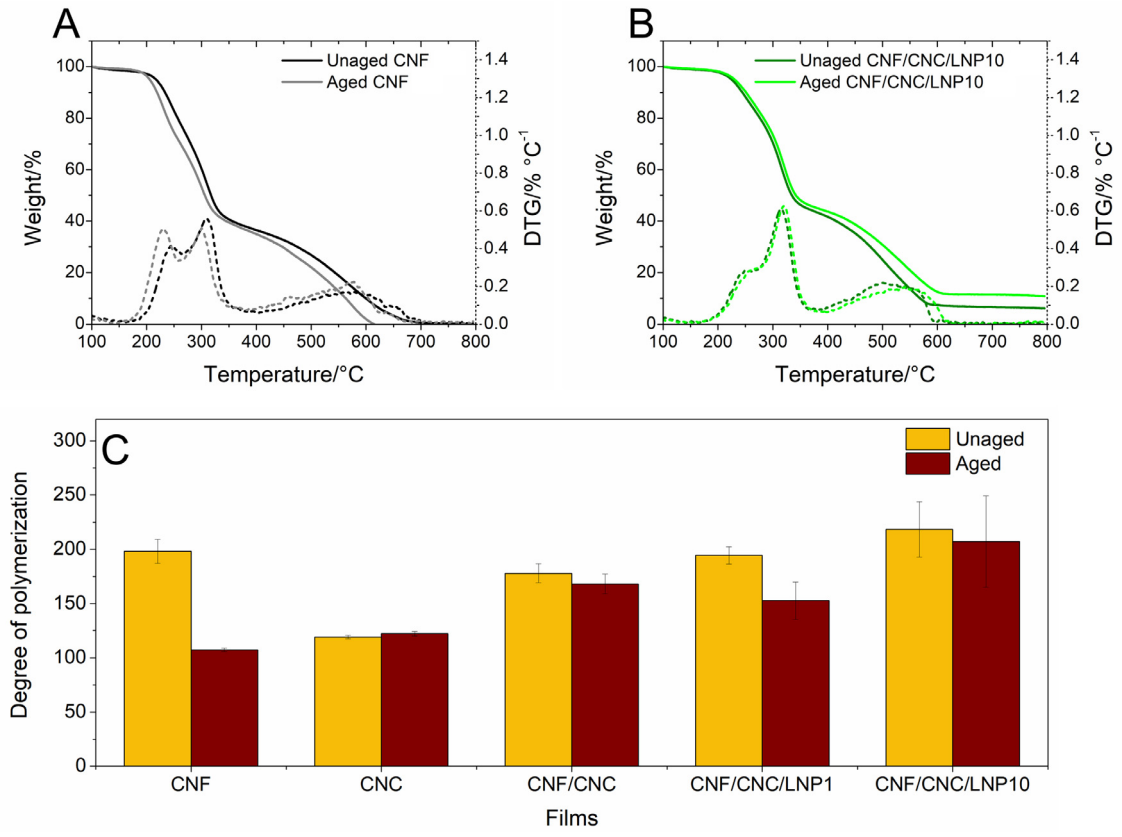

Fig. 5. TGA (left axis) and corresponding DTG curves (right axis) of unaged and aged (A) CNF and (B) CNF/CNC/LNP10 films. (C) Degree of polymerization measured for unaged and aged film samples. Moist-heat aging was performed at 80 °C and 75% RH for 168 h.

Analogously, the initial DP_v of single-component CNF film, measured as 198 ± 11 glucose units, significantly decreased to 107 ± 2 glucose units after moist-heat aging (Fig. 5C). On the other hand, the DP_v of nanocomposite films, which were statistically equivalent to that of unaged CNF film, did not significantly change after aging, nor did the DP_v of CNC film. Fukuzumi et al. [19] reported viscosimetric degree of polymerization (DP_v) values from 250 to 400 for unaged freeze-dried CNF with length-weighted average length from 200 to 1100 nm.

The reduction of cellulose DP is well reported in the literature as a result of the artificial or natural aging of cellulosic materials [50,58–60], such as paper. DP decline is an immediate effect of the hydrolysis and scission of cellulosic chains [61,62]. These phenomena usually occur simultaneously to changes in color and/or physicochemical properties, such as crystallinity.

XRD analysis showed that the crystallinity index [39] (CrI) of single-component CNF film (in duplicates) decreased from 75 ± 3% to 66 ± 3% after harsh hydrothermal aging (Fig. 6A). The CrI of CNF/CNC underwent similar reduction (79% to 70%), while the crystallinity of CNF/CNC/LNP1 reduced only slightly (73% to 70%) (Fig. S7). Two hypotheses that rationalize this behavior are depicted in Fig. 6C.

During the moist-heat aging, harsh acid hydrolysis and oxidation processes could progress until damaging [ii] the crystal ends

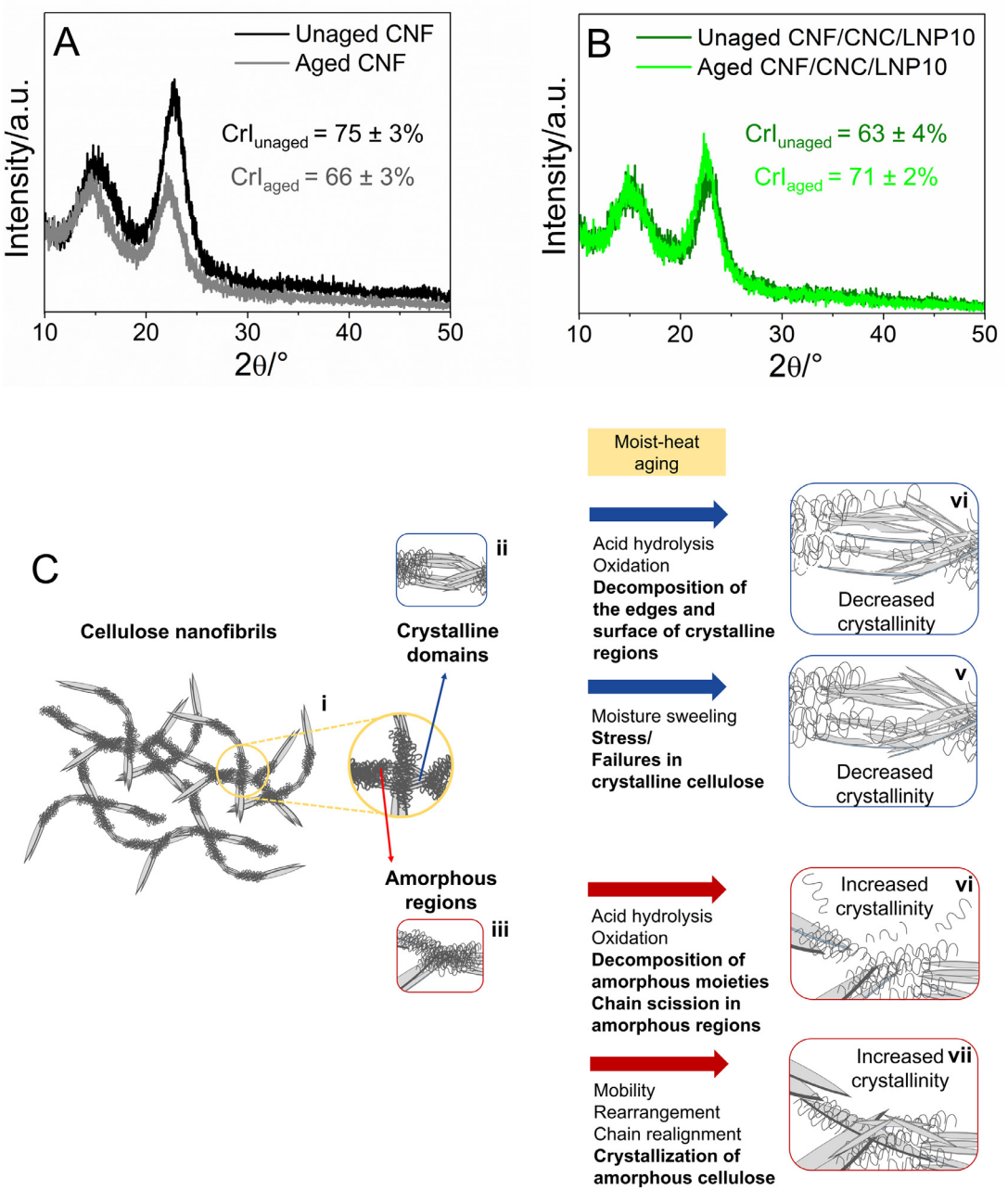

Fig. 6. X-ray diffractograms of (A) single-component CNF film and (B) CNF/CNC/LNP10 nanocomposite film before and after moist-heat aging. (C) Schematic depiction of [i] a cellulose nanofibril network with [ii] crystalline domains and [iii] amorphous regions, and the hypothesized phenomena responsible for modifying the crystallinity of the polymer: [iv] damage to cellulose chains, including on the surface and edges of crystalline domains; and [v] harsh stress and the appearance of failures in crystalline regions, both decreasing crystallinity; [vi] degradation and/or scission of cellulose chains in the amorphous regions; and [vii] the crystallization of amorphous cellulose, both increasing crystallinity.

and surfaces in the cellulose crystalline domains [62], leading to [iv] the scission of cellulose chains near the interface with amorphous segments and the reduction of the degree of polymerization (as previously observed for CNF film). Additionally, [v] defects in the crystalline domains could arise due to the severe stress of water swelling in damaged fibrils under moist conditions [63,64] or due to the formation of hydrogen bonds between amorphous and crystalline cellulose upon repeated moisture changes under high temperatures [65].

On the other hand, the CrI of CNF/CNC/LNP10 nanocomposite increased from 63 ± 4% to 71 ± 2% after moist-heat aging (Fig. 6B). Increases in crystallinity upon aging are well reported in the literature, e.g. for paper [60,62] and wood samples [66,67] under thermal and/or moisture degradation. As shown in Fig. 6C, this behavior could be explained by the [vi] favorable degradation and removal of amorphous regions in cellulose chains [62] and/or amorphous fractions in cellulose fibrils. While the degradation of amorphous zones would likely be concurrent to a decrease of DP (which was not observed for this nanocomposite), the degradation and elimination of amorphous moieties in TEMPO-oxidized CNF, especially the thermally unstable, low molecular weight sodium anhydroglucuronate units, would also contribute to a proportional increment in the crystallinity of the sample. Another hypothesis was related to the occurrence of [vii] rearrangements in the amorphous cellulose zones under high RH and temperature. The mobility and ordering of amorphous chains could promote their recrystallization

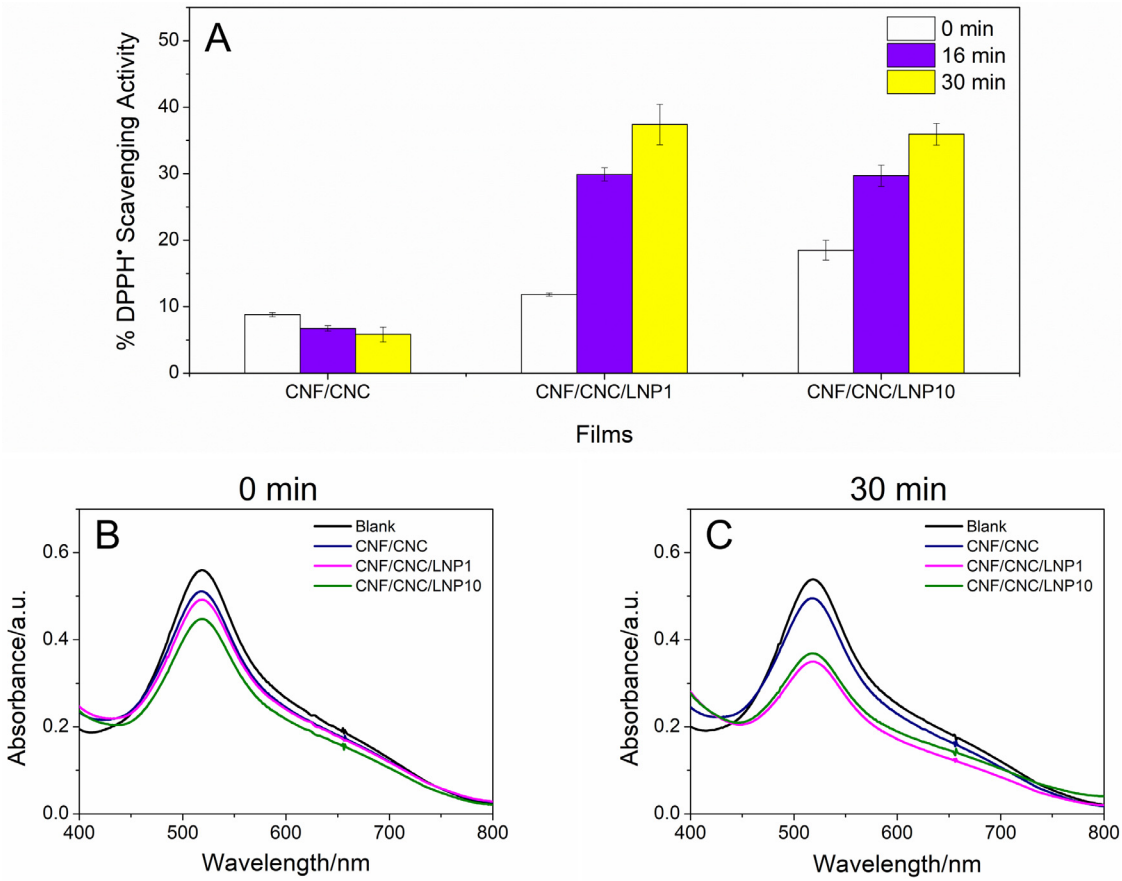

Fig. 7. Antioxidant capacity assays for the nanocomposite films. (A) % DPPH• consumption measured after 0, 16 and 30-min assays. (B,C) Representative UV-Vis absorption spectra showing the variation of the intensity of the absorption band at ~515 nm after (B) 0 min and (C) 30 min consumption or suppression of the DPPH radical in dioxane/methanol. Blank is the system containing only DPPH•, methanol, and dioxane.

[49], then increasing the CrI [65,67,68]. DSC analysis confirmed that, on the second heating step (after a first heating and controlled cooling cycle), CNF/CNC/LNP10 sample exhibited a mild but well-defined exothermic thermal event at around 88 °C, which was attributed to the recrystallization of the material (Fig. S8). The onset temperature of such thermal event was at 81 °C for the unaged sample, being consistent with the increased crystallinity observed for this film when it was aged at 80 °C for 168 h. The recrystallization is associated with the phenomenon of reorganization of amorphous polymer chains to form a more stable crystalline structure during heating [69]. This result indicates that the increase in sample crystallinity is probably a consequence of the concurrent removal of amorphous components and recrystallization of cellulosic chains that compose the films.

Therefore, the results of colorimetric, thermal, DP, and XRD analyses reported here have provided a comprehensive assessment of the influence of the degradation of TEMPO-oxidized CNF on the stability of composite systems in which this nanocellulosic material is only one of multiple components.

3.4. Role of antioxidant capacity of nanolignin in mitigating the degradation of nanocellulose-based nanocomposites

LNP-containing nanocomposite films showed improved colorimetric, thermal, and physicochemical stability than single-component CNF film. In addition to the presence of highly chemically resistant CNC, this enhanced physicochemical behavior could be mainly attributed to the presence of LNP.

The presence of lignin in cellulosic materials, such as modern paper, has historically been considered as a deterioration-inducing factor due to the production of acid species during the degradation and oxidation of this aromatic macromolecule [53,58,70]. Nevertheless, researchers such as Bégin et al. [71] and Małachowska et al. [61] demonstrated that lignin has no negative effect on the deterioration of paper at neutral pH. In fact, even though lignin is vulnerable to photo-oxidation [61], it can also mitigate or inhibit the oxidation of cellulosic materials due to its antioxidant capacity [57,72].

DPPH radical scavenging activity was measured to evaluate the antioxidant capability of LNP, which could contribute to the stability of nanocomposites during moist-heat aging (Fig. 7A). Measurements were performed using the films, so that the antioxidant capacity of the lignin trapped on the surface of intact films was assessed directly, not that of the lignin in solution or dispersion, as conventionally reported by other studies [29,42]. Instantaneous consumption of the free radical, with significant reduction in the relative absorbance at 515 nm, was verified immediately after contact between DPPH• in dioxane/methanol solution and LNP-containing nanocomposite films (Fig. 7B). Scavenging effect was significantly higher for CNF/CNC/LNP10 as compared to CNF/CNC/LNP1 and CNF/CNC. After 16 and 30-min contact assays the antioxidant capacity of the nanocomposite films containing 1 and 10% (w/w) LNP increased from 12% and 18%, respectively, to around 30–40% (Fig. 7C). The same assay performed in a greener manner, using only ethanol as solvent, showed similar results (Fig. S9). Such values are comparable to DPPH• scavenging activity reported for edible methylcellulose films incorporated with

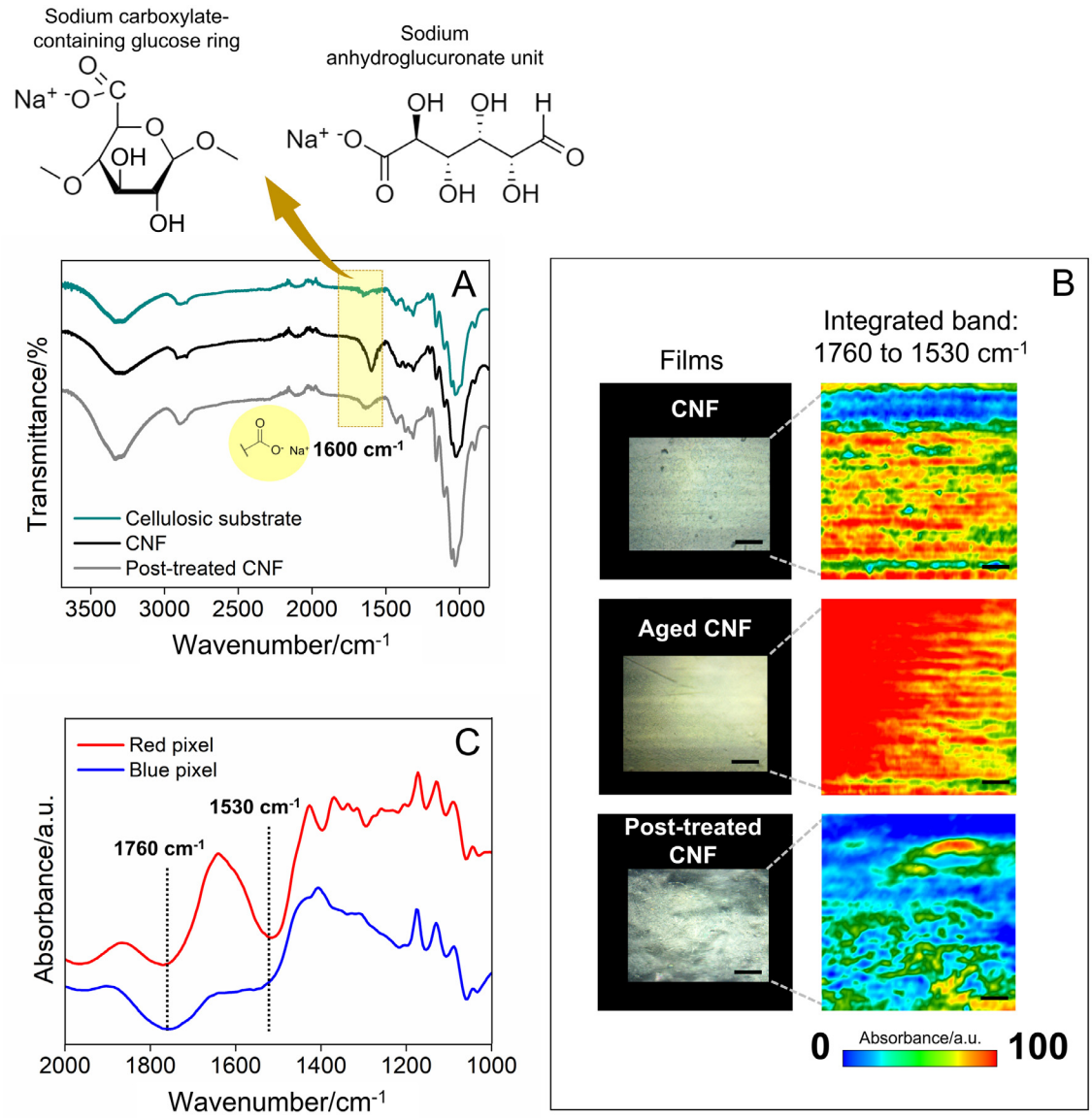

Fig. 8. (A) ATR-FTIR spectra for starting cellulosic substrate and CNF and post-treated CNF films. Yellow box indicates the absorption band at about 1600 cm^{-1} and the chemical structures of sodium carboxylate-containing glucose and anhydroglucuronate unit are depicted above. (B) Optical micrographs under visible light (left) and micro-FTIR 2D maps (right) collected in different random regions of CNF, aged CNF, and post-treated CNF film. Scale bars: 200 μm. False color scale: lowest intensity of the integrated band (1760–1530 cm^{-1}) in blue and highest intensity in red. (C) FTIR spectra corresponding to a representative blue and red pixel collected using micro-FTIR. The spatial resolution of the equipment is 5.5 μm, i.e., each pixel corresponds to a sample area of about 30 μm^2.

α-tocopherol (vitamin E). Films containing 30, 50, and 70% (w/w) of this well-known and strong antioxidant showed antioxidant capacity of around 33%, 43%, and 56%, respectively [41].

The good antioxidant performance of CNF/CNC/LNP1 and CNF/CNC/LNP10 certainly contributed to the higher stability of these nanocomposites against degradation. As the progression of the measured scavenging effect prevails onto the surface of the films only, the antioxidant capabilities assessed for these two different nanocomposites were not concentration-dependent over times longer than 16 min. However, the presence of higher concentration of LNP on the film surface and inner structure promoted a consistent antioxidant performance for the nanocomposite containing 10% (w/w) LNP, whose radical scavenging activity was the highest from the start. In fact, the synergistic effects of moist-heat aging implied just minor color and physicochemical changes in this sample. This result agrees with previously reported studies in which small amounts of antioxidant lignin (1% w/w) were added to polymeric matrices to improve their thermal stability and resistance to photo-oxidation [73]. Therefore, the intrinsic antioxidant properties of lignin make this phenolic macromolecule a natural and cheap ally to produce stable nanocomposites, avoiding the need for extra antioxidant species, such as butylated hydroxyanisole (BHA) or ascorbic acid [29].

3.5. Improving the colorimetric and thermal stability by removing chemically unstable groups

Previous discussion evidenced the contribution of the incorporation of LNP to the stability of nanocomposite films subjected to moist-heat aging. In addition, the characterization conducted for single-component CNF film also showed its high susceptibility to degradation.

As discussed before, TEMPO-oxidized CNF usually contain thermally unstable sodium anhydroglucuronate units and sodium carboxylate groups [9,25,27]. FTIR spectra in Fig. 8A shows the rise of an absorption band around 1600 cm^{-1} assigned to the intro-

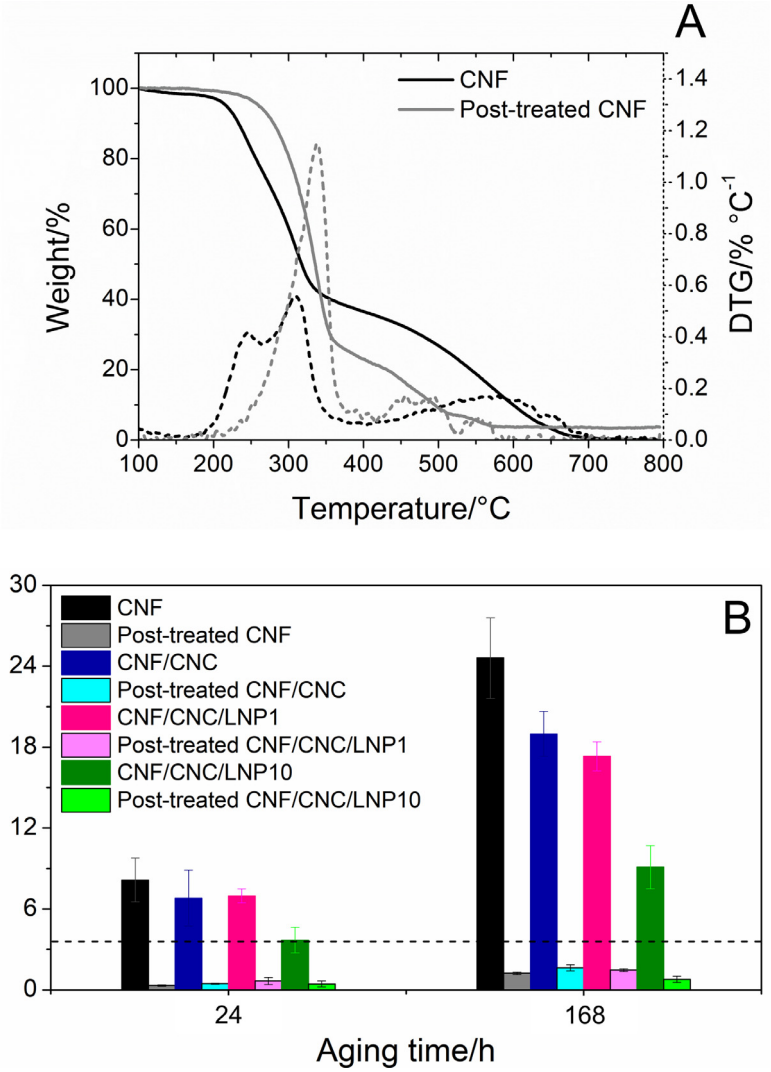

Fig. 9. (A) Curves of TGA (left axis) and corresponding DTG (right axis) for the post-treated CNF film in comparison to an untreated CNF film. (B) ΔE calculated for the post-treated CNF and nanocomposite films made with these CNF after moist-heat aging for 24 and 168 h. Dotted line demarcates the value of 3.5 on the ordinate axis. Results for untreated CNF were included for comparison.

duction of these functional groups onto cellulose after TEMPO-mediated oxidation [74]. Therefore, removing those structural triggers of degradation could cooperate to improve CNF stability. To this end, a sequential post-treatment [25] using 1 mol L^{-1} NaOH and 0.1 mol L^{-1} HCl was carried out. The first alkali hydrothermal step eliminated anhydroglucuronate residues, while the second acid step converted sodium carboxylate into free carboxyl groups.

As shown in the FTIR spectrum of post-treated CNF film, there was a significant decrease in the relative intensity of the adsorption band assigned to sodium carboxylate (Fig. 8A). Moreover, micro-FTIR 2D mapping (Fig. 8B, C) also evidenced a high spatial distribution of these functional groups in unaged and aged CNF films, while the intensity of the integrated band (1760 to 1530 cm^{-1}) decreased after the post-treatment.

The surface charge density of TEMPO-oxidized CNF dropped by around 45% after the post-treatments. Accordingly, TGA and DTG curves (Fig. 9A) confirmed the enhancement of the thermal stability of CNF film. The broader DTG curve for CNF film, with an initial DTG_{peak} around 243 °C, was replaced by a narrower maximum DTG_{peak} at 337 °C for post-treated CNF film. Likewise, nanocomposite films prepared with post-treated CNF, which exhibited visual aspect and colorimetric parameters virtually equivalent to those of untreated films (Figs. S10 and S11), presented higher T_d and DTG_{peak} than their untreated analogues (Fig. S12).

The DP_v of the post-treated sample was 291 ± 32 monomers, superior to the DP_v of untreated sample (198 ± 11) probably due to the removal of some low molecular weight sodium anhydroglucuronate units previously adsorbed on the longer TEMPO-CNF. Moreover, the absence of these unstable groups likely prevented the occurrence of β-elimination reactions and CNF depolymerization during the dissolution in CED for DP_v measurements [26].

When post-treated CNF underwent moist-heat aging for 24 or 168 h, both the ΔE and L*a*b* variations were negligible and statistically equivalent for all samples, including nanocomposites (Fig. 9B and S13). The DP_v of post-treated CNF sample also remained constant after aging for 168 h (300 ± 8 monomers), indicating absence of further chain scissions. Therefore, the alkali-acid post-treatment was another efficient strategy to improve the thermal, colorimetric, and structural stability of single-component CNF, pairing its performance to that of nanolignin-containing nanocomposites.

Although previous publications have already revealed the contribution of sodium carboxylate groups and sodium anhydroglucuronate units to the lack of thermal stability of TEMPO-oxidized

[25], the results presented here shed new light on the simultaneous negative effects of these chemical moieties on the physicochemical and colorimetric stability of nanocelluloses.

4. Conclusion

Two strategies were carried out in parallel to improve the stability of TEMPO-oxidized cellulose nanofibrils and nanocellulose-based nanocomposites. Single-component CNF systems are very susceptible to colorimetric, thermal, and physicochemical degradation during moist-heat aging. As a greener approach, the incorporation of lignin nanoparticles with high antioxidant activity contributed to mitigate the synergistic effects of high temperature and relative humidity on the nanocomposite films. As a parallel strategy, an alkali-acid post-treatment was effective in removing unstable functional groups and residues from CNF, improving the aging resistance and revealing the remarkable contribution of sodium carboxylate moieties to the prior instability of untreated CNF. Both approaches, the implementation of a post-treatment and the incorporation of LNP, can potentially cooperate for the development of stable, durable, highly antioxidant, and UV-protective nanocomposites. The different methods were confirmed to be complementary to some extent, as nanocomposite films made of post-treated CNF presented high colorimetric and thermal stability, but the decision to use them separately should be made with different target outcomes in mind. When CNF are expected to be applied alone or in colorless/highly transparent systems, post-treatment is likely the best option. Nevertheless, the demand for high temperature and relatively concentrated alkali and acid solutions are drawbacks of this method. On the other hand, incorporating LNP would be a greener and sustainable alternative without the need for additional chemical reactions, but nanolignin natural color and the formation of nanocomposite systems must be considered.

Appendix

Supplementary data includes: measurements of film thickness; experimental apparatus of artificially-accelerated aging; photos of films aged at 40 and 80 °C with varied RH for 168 h; variation of colorimetric parameters of the films due to artificially-accelerated aging; reaction schemes and mechanisms for cellulose degradation and stabilization; ΔE for binary CNF/LNP and CNC/LNP films; TGA analysis of unaged and aged films; XRD analysis; DSC analysis; DPPH radical scavenging activity of the nanocomposites in ethanol; photos of post-treated CNF and post-treated CNF-based nanocomposites; TGA and DTG curves of post-treated CNF nanocomposite films; colorimetric parameters of post-treated CNF films; variation of colorimetric parameters of the post-treated CNF films due to moist-heat aging.

Declaration of Competing Interest

The authors declare that they have no known competing financial interests or personal relationships that could have appeared to influence the work reported in this paper.

Acknowledgements

We acknowledge IQ-UNICAMP and CSGI/Di partimento di Chimica 'Ugo Schiff' - UniFI for providing infrastructure and access to analysis apparatus. We thank Dr. Douglas Soares (*in memorian*) for the support and help during TEM analysis and lab activities. Financial support was granted by São Paulo Research Foundation (FAPESP, grant 2018/23769-1), National Council for Scientific and Technological Development (CNPq, grants 140558/2017-9 and 420031/2018-9), Coordenação de Aperfeiçoamento de Pessoal de Nível Superior – Brazil (CAPES, financial code 001), and Ministero degli Affari Esteri e della Cooperazione Internazionale (Italy).

Supplementary materials

Supplementary material associated with this article can be found, in the online version, at doi:10.1016/j.polymdegradstab.2022.109943.

References

[1] A. Isogai, T. Saito, H. Fukuzumi, TEMPO-oxidized cellulose nanofibers, Nanoscale 3 (2011) 71–85, doi:10.1039/c0nr00583e.
[2] G. Siqueira, J. Bras, A. Dufresne, Cellulosic Bionanocomposites: A Review of Preparation, Properties and Applications, Polymers (Basel) 2 (2010) 728–765, doi:10.3390/polym2040728.
[3] Q. Tarrés, M. Delgado-Aguilar, M.A. Pèlach, I. González, S. Boufi, P. Mutjé, Remarkable increase of paper strength by combining enzymatic cellulose nanofibers in bulk and TEMPO-oxidized nanofibers as coating, Cellulose 23 (2016) 3939–3950, doi:10.1007/s10570-016-1073-0.
[4] M. Kluge, S. Veigel, S. Pinkl, U. Henniges, C. Zollfrank, A. Rössler, W. Gindl-Altmutter, Nanocellulosic fillers for waterborne wood coatings: reinforcement effect on free-standing coating films, Wood Sci. Technol. 51 (2017) 601–613, doi:10.1007/s00226-017-0892-y.
[5] C.H.M. Camargos, J.C.D. Figueiredo, F.V. Pereira, Cellulose nanocrystal-based composite for restoration of lacunae on damaged documents and artworks on paper, J. Cult. Herit. 23 (2017) 170–175, doi:10.1016/j.culher.2016.10.007.
[6] K. Kolman, O. Nechyporchuk, M. Persson, K. Holmberg, R. Bordes, Combined Nanocellulose/Nanosilica Approach for Multiscale Consolidation of Painting Canvases, ACS Appl. Nano Mater. 1 (2018) 2036–2040, doi:10.1021/acsanm.8b00262.
[7] C. Cianci, D. Chelazzi, G. Poggi, F. Modi, R. Giorgi, M. Laurati, Hybrid fibroin-nanocellulose composites for the consolidation of aged and historical silk, Colloids Surfaces A Physicochem. Eng. Asp. 634 (2022) 127944, doi:10.1016/J.COLSURFA.2021.127944.
[8] N. Lavoine, I. Desloges, A. Dufresne, J. Bras, Microfibrillated cellulose - Its barrier properties and applications in cellulosic materials: A review, Carbohydr. Polym. 90 (2012) 735–764, doi:10.1016/j.carbpol.2012.05.026.
[9] H. Fukuzumi, T. Saito, T. Iwata, Y. Kumamoto, A. Isogai, Transparent and high gas barrier films of cellulose nanofibers prepared by TEMPO-mediated oxidation, Biomacromolecules 10 (2009) 162–165, doi:10.1021/bm801065u.
[10] V.T. Noronha, C.H.M. Camargos, J.C. Jackson, A.G. Souza Filho, A.J. Paula, C.A. Rezende, A.F. Faria, Physical Membrane-Stress-Mediated Antimicrobial Properties of Cellulose Nanocrystals, ACS Sustain. Chem. Eng. 9 (2021) 3203–3212, doi:10.1021/acssuschemeng.0c08317.
[11] J.C. Jackson, C.H.M. Camargos, V.T. Noronha, A.J. Paula, C.A. Rezende, A.F. Faria, Sustainable Cellulose Nanocrystals for Improved Antimicrobial Properties of Thin Film Composite Membranes, ACS Sustain. Chem. Eng. 9 (2021) 6534–6540, doi:10.1021/acssuschemeng.1c02389.
[12] H. Zhu, Z. Fang, C. Preston, Y. Li, L. Hu, Transparent paper: Fabrications, properties, and device applications, Energy Environ. Sci. 7 (2014) 269–287, doi:10.1039/c3ee43024c.
[13] H. Du, W. Liu, M. Zhang, C. Si, X. Zhang, B. Li, Cellulose nanocrystals and cellulose nanofibrils based hydrogels for biomedical applications, Carbohydr. Polym. 209 (2019) 130–144, doi:10.1016/j.carbpol.2019.01.020.
[14] O. Nechyporchuk, M.N. Belgacem, J. Bras, Production of cellulose nanofibrils: A review of recent advances, Ind. Crops Prod. 93 (2016) 2–25, doi:10.1016/j.indcrop.2016.02.016.
[15] L.O. Pinto, J.S. Bernardes, C.A. Rezende, Low-energy preparation of cellulose nanofibers from sugarcane bagasse by modulating the surface charge density, Carbohydr. Polym. 218 (2019) 145–153, doi:10.1016/j.carbpol.2019.04.070.
[16] J. Milanovic, T. Lazic, I. Zivkovic, M. Vuksanovic, M. Milosevic, M. Kostic, The Effect of Nanofibrillated Tempo-oxidized Cotton Linters on the Strength and Optical Properties of Paper, J. Nat. Fibers. (2020), doi:10.1080/15440478.2020.1848742.
[17] T. Kasuga, H. Yagyu, K. Uetani, H. Koga, M. Nogi, Cellulose Nanofiber Coatings on Cu Electrodes for Cohesive Protection against Water-Induced Short-Circuit Failures, ACS Appl. Nano Mater 4 (2021) 3861–3868, doi:10.1021/ACSANM.1C00267.
[18] M. El Bakkari, V. Bindiganavile, Y. Boluk, Facile Synthesis of Calcium Hydroxide Nanoparticles onto TEMPO-Oxidized Cellulose Nanofibers for Heritage Conservation, ACS Omega 4 (2019) 20606–20611, doi:10.1021/acsomega.9b02643.
[19] H. Fukuzumi, T. Saito, A. Isogai, Influence of TEMPO-oxidized cellulose nanofibril length on film properties, Carbohydr. Polym. 93 (2013) 172–177, doi:10.1016/j.carbpol.2012.04.069.
[20] A. Isogai, T. Saito, US 8992728 B2 - Cellulose nanofiber, production method of same and cellulose nanofiber dispersion, 2015. https://patents.google.com/patent/US8992728B2/en (accessed July 19, 2021).
[21] S. Takaichi, T. Saito, R. Tanaka, A. Isogai, Improvement of nanodispersibility of oven-dried TEMPO-oxidized celluloses in water, Cellulose 21 (2014) 4093–4103, doi:10.1007/s10570-014-0444-7.

[22] J. Xia, Z. Zhang, W. Liu, V.C.F. Li, Y. Cao, W. Zhang, Y. Deng, Highly transparent 100% cellulose nanofibril films with extremely high oxygen barriers in high relative humidity, Cellulose 25 (2018) 4057–4066, doi:10.1007/s10570-018-1843-y.
[23] S.P. Mishra, A.S. Manent, B. Chabot, C. Daneault, The use of sodium chlorite in post-oxidation of TEMPO-oxidized pulp: Effect on pulp characteristics and nanocellulose yield, J. Wood Chem. Technol. 32 (2012) 137–148, doi:10.1080/02773813.2011.624666.
[24] K. Lichtenstein, N. Lavoine, Toward a deeper understanding of the thermal degradation mechanism of nanocellulose, Polym. Degrad. Stab. 146 (2017) 53–60, doi:10.1016/j.polymdegradstab.2017.09.018.
[25] H. Fukuzumi, T. Saito, Y. Okita, A. Isogai, Thermal stabilization of TEMPO-oxidized cellulose, Polym. Degrad. Stab. 95 (2010) 1502–1508, doi:10.1016/j.polymdegradstab.2010.06.015.
[26] R. Shinoda, T. Saito, Y. Okita, A. Isogai, Relationship between length and degree of polymerization of TEMPO-oxidized cellulose nanofibrils, Biomacromolecules 13 (2012) 842–849, doi:10.1021/bm2017542.
[27] N. Lavoine, J. Bras, T. Saito, A. Isogai, Improvement of the Thermal Stability of TEMPO-Oxidized Cellulose Nanofibrils by Heat-Induced Conversion of Ionic Bonds to Amide Bonds, Macromol. Rapid Commun. 37 (2016) 1033–1039, doi:10.1002/marc.201600186.
[28] C.H.M. Camargos, C.A. Rezende, Structure-Property Relationships of Cellulose Nanocrystals and Nanofibrils: Implications for the Design and Performance of Nanocomposites and All-Nanocellulose Systems, ACS Appl. Nano Mater 4 (2021) 10505–10518, doi:10.1021/acsanm.1c02008.
[29] C.H.M. Camargos, C.A. Rezende, Antisolvent versus ultrasonication: Bottom-up and top-down approaches to produce lignin nanoparticles (LNPs) with tailored properties, Int. J. Biol. Macromol. 193 (2021) 647–660, doi:10.1016/j.ijbiomac.2021.10.094.
[30] O. Cusola, O.J. Rojas, M.B. Roncero, Lignin Particles for Multifunctional Membranes, Antioxidative Microfiltration, Patterning, and 3D Structuring, ACS Appl. Mater. Interfaces. 11 (2019) 45226–45236, doi:10.1021/acsami.9b16931.
[31] M. Farooq, T. Zou, G. Riviere, M.H. Sipponen, M. Österberg, Strong, Ductile, and Waterproof Cellulose Nanofibril Composite Films with Colloidal Lignin Particles, Biomacromolecules 20 (2019) 693–704, doi:10.1021/acs.biomac.8b01364.
[32] M. Parit, P. Saha, V.A. Davis, Z. Jiang, Transparent and Homogenous Cellulose Nanocrystal/Lignin UV-Protection Films, ACS Omega 3 (2018) 10679–10691, doi:10.1021/acsomega.8b01345.
[33] C.F. Forney, D.G. Brandl, Control of Humidity in Small Controlled-environment Chambers using Glycerol-Water Solutions, Horttechnology 2 (1992) 52–54, doi:10.21273/horttech.2.1.52.
[34] S.A.A.K.M. Hamed, M.L. Hassan, A new mixture of hydroxypropyl cellulose and nanocellulose for wood consolidation, J. Cult. Herit. 35 (2019) 140–144, doi:10.1016/j.culher.2018.07.001.
[35] ISO 5630-2, Paper and board - Accelerated ageing. Part 2: Moist heat treatment at 90 °C and 25% relative humidity, 1985. https://www.iso.org/standard/11710.html (accessed April 8, 2021).
[36] W.S. Mokrzycki, M. Tatol, Color difference ΔE - A survey, Mach. Graph. Vis. 20 (2011) 383–411.
[37] ISO 5351, Pulps - Determination of limiting viscosity number in cupri-ethylenediamine (CED) solution, 1199 (2010) 23. https://www.iso.org/standard/51093.html (accessed April 11, 2021).
[38] M. Henriksson, L.A. Berglund, P. Isaksson, T. Lindström, T. Nishino, Cellulose nanopaper structures of high toughness, Biomacromolecules 9 (2008) 1579–1585, doi:10.1021/bm800038n.
[39] L. Segal, J.J. Creely, A.E. Martin, C.M. Conrad, An Empirical Method for Estimating the Degree of Crystallinity of Native Cellulose Using the X-Ray Diffractometer, Text. Res. J. 29 (1959) 786–794, doi:10.1177/004051755902901003.
[40] X. Pan, J.F. Kadla, K. Ehara, N. Gilkes, J.N. Saddler, Organosolv ethanol lignin from hybrid poplar as a radical scavenger: Relationship between lignin structure, extraction conditions, and antioxidant activity, J. Agric. Food Chem. 54 (2006) 5806–5813, doi:10.1021/jf0605392.
[41] C.M. Noronha, S.M. de Carvalho, R.C. Lino, P.L.M. Barreto, Characterization of antioxidant methylcellulose film incorporated with α-tocopherol nanocapsules, Food Chem 159 (2014) 529–535, doi:10.1016/J.FOODCHEM.2014.02.159.
[42] H. Trevisan, C.A. Rezende, Pure, stable and highly antioxidant lignin nanoparticles from elephant grass, Ind. Crops Prod. 145 (2020) 112105, doi:10.1016/j.indcrop.2020.112105.
[43] W.G. Glasser, About Making Lignin Great Again—Some Lessons From the Past, Front. Chem. 7 (2019) 565, doi:10.3389/fchem.2019.00565.
[44] R.J. Moon, A. Martini, J. Nairn, J. Simonsen, J. Youngblood, Cellulose nanomaterials review: structure, properties and nanocomposites, Chem. Soc. Rev. 40 (2011) 3941–3994, doi:10.1039/C0CS00108B.
[45] T. Vitale, D. Erhardt, Changes in paper color due to artificial aging and the effects of washing on color removal, in: ICOM Comm, Conserv. z, Washington, DC, 1993, pp. 507–515. 22-27 August 1993 Prepr..
[46] E.L. Graminski, E.J. Parks, E.E. Toth, The Effects of Temperature and Moisture on the Accelerated Aging of Paper, Restaurator. 2 (1978) 175–178. doi:10.1515/rest.1978.2.3.175.
[47] A. Schedl, T. Zweckmair, F. Kikul, U. Henniges, T. Rosenau, A. Potthast, Aging of paper – Ultra-fast quantification of 2,5-dihydroxyacetophenone, as a key chromophore in cellulosics, by reactive paper spray-mass spectrometry, Talanta 167 (2017) 672–680, doi:10.1016/J.TALANTA.2017.02.053.
[48] T. Łojewski, P. Miśkowiec, M. Missori, A. Lubańska, L.M. Proniewicz, J. Łojewska, FTIR and UV/vis as methods for evaluation of oxidative degradation of model paper: DFT approach for carbonyl vibrations, Carbohydr. Polym. 82 (2010) 370–375, doi:10.1016/j.carbpol.2010.04.087.
[49] E. Małachowska, D. Pawcenis, J. Dańczak, J. Paczkowska, K. Przybysz, Paper ageing: The effect of paper chemical composition on hydrolysis and oxidation, Polymers (Basel). 13 (2021). https://doi.org/ 10.3390/polym13071029.
[50] S. Zervos, Natural and accelerated ageing of cellulose and paper: A literature review, in: Cellul. Struct. Prop. Deriv. Ind. Uses, Nova Science Publishers, 2010, pp. 1–42.
[51] K. Ahn, S. Zaccaron, N.S. Zwirchmayr, H. Hettegger, A. Hofinger, M. Bacher, U. Henniges, T. Hosoya, A. Potthast, T. Rosenau, Yellowing and brightness reversion of celluloses: CO or COOH, who is the culprit? Cellulose 26 (2019) 429–444, doi:10.1007/s10570-018-2200-x.
[52] T. Rosenau, A. Potthast, K. Krainz, Y. Yoneda, T. Dietz, Z.P.I. Shields, A.D. French, Chromophores in cellulosics, VI. First isolation and identification of residual chromophores from aged cotton linters, Cellulose. 18 (2011) 1623–1633. https://doi.org/ 10.1007/S10570-011-9585-0/FIGURES/6.
[53] M. Strlič, J. Kolar, Ageing and stabilisation of paper, National and University Library, Ljubljana, 2005.
[54] T. Łojewski, K. Zięba, A. Knapik, J. Bagniuk, A. Lubańska, J. Łojewska, Evaluating paper degradation progress. Cross-linking between chromatographic, spectroscopic and chemical results, Appl. Phys. A Mater. Sci. Process. 100 (2010) 809–821, doi:10.1007/s00339-010-5657-5.
[55] A. Potthast, T. Rosenau, P. Kosma, Analysis of Oxidized Functionalities in Cellulose (2006) 1–48 Adv. Polym. Sci., doi:10.1007/12_099.
[56] A. Potthast, K. Ahn, M. Becker, T. Eichinger, M. Kostic, S. Böhmdorfer, M.J. Jeong, T. Rosenau, Acetylation of cellulose – Another pathway of natural cellulose aging during library storage of books and papers, Carbohydr. Polym. 287 (2022) 119323, doi:10.1016/j.carbpol.2022.119323.
[57] J.A. Schmidt, C.S. Rye, N. Gurnagul, Lignin inhibits autoxidative degradation of cellulose, Polym. Degrad. Stab. 49 (1995) 291–297, doi:10.1016/0141-3910(95)87011-3.
[58] A.L. Dupont, C. Egasse, A. Morin, F. Vasseur, Comprehensive characterisation of cellulose- and lignocellulose-degradation products in aged papers: Capillary zone electrophoresis of low-molar mass organic acids, carbohydrates, and aromatic lignin derivatives, Carbohydr. Polym. 68 (2007) 1–16, doi:10.1016/j.carbpol.2006.07.005.
[59] A. Emsley, R.J. Heywood, M. Ali, C. Eley, On the kinetics of degradation of cellulose, Cellulose 4 (1997) 1–5, doi:10.1023/A:1018408515574.
[60] X. Zou, N. Gurnagul, T. Uesaka, J. Bouchard, Accelerated aging of papers of pure cellulose: mechanism of cellulose degradation and paper embrittlement, Polym. Degrad. Stab. 43 (1994) 393–402, doi:10.1016/0141-3910(94)90011-6.
[61] E. Małachowska, M. Dubowik, P. Boruszewski, J. Łojewska, P. Przybysz, Influence of lignin content in cellulose pulp on paper durability, Sci. Rep. (2020) 10, doi:10.1038/s41598-020-77101-2.
[62] C.H. Stephens, P.M. Whitmore, H.R. Morris, M.E. Bier, Hydrolysis of the amorphous cellulose in cotton-based paper, Biomacromolecules 9 (2008) 1093–1099, doi:10.1021/bm800049w.
[63] W. Mo, K. Ke, X. Shen, B. Li, The influence of "thermal drying pretreatment" on enzymatic hydrolysis of cellulose and xylan in poplar fibers with high lignin content, Carbohydr. Polym. (2020) 228, doi:10.1016/j.carbpol.2019.115400.
[64] H.L. Needles, K.C.J. Nowak, Heat-induced ageing of linen, ACS Symp. Ser. (1988) 159–167 Hist. Text. Pap. Mater. 2.1990, doi:10.1021/bk-1989-0410.ch011.
[65] A. Tarmian, A. Mastouri, Changes in moisture exclusion efficiency and crystallinity of thermally modified wood with aging, IForest 12 (2019) 92–97, doi:10.3832/ifor2723-011.
[66] F. Lionetto, R. Del Sole, D. Cannoletta, G. Vasapollo, A. Maffezzoli, Monitoring Wood Degradation during Weathering by Cellulose Crystallinity, Materials (Basel) 5 (2012) 1910–1922, doi:10.3390/ma5101910.
[67] M.T.R. Bhuiyan, N. Hirai, N. Sobue, Changes of crystallinity in wood cellulose by heat treatment under dried and moist conditions, J. Wood Sci. 46 (2000) 431–436, doi:10.1007/BF00765800.
[68] M. Tyufekchiev, A. Kolodziejczak, P. Duan, M. Foston, K. Schmidt-Rohr, M.T. Timko, Reaction engineering implications of cellulose crystallinity and water-promoted recrystallization, Green Chem 21 (2019) 5541–5555, doi:10.1039/c9gc02466b.
[69] Y. Furushima, C. Schick, A. Toda, Crystallization, recrystallization, and melting of polymer crystals on heating and cooling examined with fast scanning calorimetry, Polym. Cryst. 1 (2018) e10005, doi:10.1002/PCR2.10005.
[70] C. Fellers, T. Iversen, T. Lindstrom, T. Nilsson, M. Rigdahl, Ageing/degradation of paper, a literature survey, FoU- Proj. Papperskonservering. (1989).
[71] P. Bégin, S. Deschâtelets, D. Grattan, N. Gurnagul, J. Iraci, E. Kaminska, D. Woods, X. Zou, The Impact of Lignin on Paper. Permanence A Comprehensive Study of the Ageing Behaviour of Handsheets and Commercial Paper Samples, Restaurator 19 (1998) 135–154.
[72] E. Vänskä, T. Vihelä, M.S. Peresin, J. Vartiainen, M. Hummel, T. Vuorinen, Residual lignin inhibits thermal degradation of cellulosic fiber sheets, Cellulose 23 (2016) 199–212, doi:10.1007/s10570-015-0791-z.
[73] C. Pouteau, P. Dole, B. Cathala, L. Averous, N. Boquillon, Antioxidant properties of lignin in polypropylene, Polym. Degrad. Stab. 81 (2003) 9–18, doi:10.1016/S0141-3910(03)00057-0.
[74] S. Coseri, G. Biliuta, L.F. Zemljič, J.S. Srndovic, P.T. Larsson, S. Strnad, T. Kreže, A. Naderi, T. Lindström, One-shot carboxylation of microcrystalline cellulose in the presence of nitroxyl radicals and sodium periodate, RSC Adv 5 (2015) 85889–85897, doi:10.1039/c5ra16183e.